AIP | Applied Physics Letters

Hypersonic acoustic mirrors and microcavities in porous silicon

G. N. Aliev, B. Goller, D. Kovalev, and P. A. Snow

Citation: Appl. Phys. Lett. **96**, 124101 (2010); doi: 10.1063/1.3367747
View online: http://dx.doi.org/10.1063/1.3367747
View Table of Contents: http://apl.aip.org/resource/1/APPLAB/v96/i12
Published by the American Institute of Physics.

Hypersonic acoustic mirrors and microcavities in porous silicon

G. N. Aliev,[a] B. Goller, D. Kovalev, and P. A. Snow
Department of Physics, University of Bath, Bath BA2 7AY, United Kingdom

(Received 7 February 2010; accepted 27 February 2010; published online 22 March 2010)

Periodic solid state structures exhibit transmission stop bands for waves of certain frequencies. We report the realization and direct measurement of acoustic band gaps in porous silicon multilayer structures which exhibit ~50 dB stop bands for longitudinal acoustic waves in the gigahertz range. Furthermore, realization of an acoustic microcavity structure in porous silicon is demonstrated.
 [doi:10.1063/1.3367747]

Porous silicon (pSi) is known as a versatile material with applications in light emission, sensing, and photonic crystal devices.[1] The possibility of producing acoustic band gaps in pSi was proposed in 2005.[2] Detailed calculations of predicted bandwidths were subsequently published.[3,4] Recently, experimental results of Brillouin light scattering suggested the existence of zone-folded phonons and phononic band gaps in pSi multilayers.[5] Here, we report the realization of hypersonic band gaps and microcavities in pSi multilayer structures observed by direct measurement of transmission spectra for longitudinal acoustic waves.

In optics, a distributed Bragg reflector (DBR) consists of a number of repeated layer pairs where each pair consists of a layer of thickness d_1 having refractive index n_1 followed by a layer of thickness d_2 with index n_2. The reflectivity of the mirror is determined by the number of repeating pairs and by the refractive index contrast between the layer materials. The strong reflectivity profile—the optical band gap—appears around the Bragg wavelength λ_B (in vacuum) given for normal incidence by the following:

$$m\lambda_B/2 = n_1 d_1 + n_2 d_2, \quad m = 1,2,3\ldots, \tag{1}$$

where m is the order number for the multiple stop bands.

For acoustic waves in a periodic structure, the situation is similar; the mismatch in the acoustic impedance between layers results in waves that are reflected and interfere. The expression for the center of frequency stop bands f_B of the different orders m in an acoustic Bragg mirror for normal incidence can be written as follows:

$$2f_B/m = (\rho_1 d_1/Z_1 + \rho_2 d_2/Z_2)^{-1}, \quad m = 1,2,3\ldots, \tag{2}$$

where the layer thicknesses are represented by d_i as before, and Z_1 and Z_2 are the acoustic impedances of the alternating layers. The acoustic impedance Z of any layer is given by ρV, where V is the sound velocity and ρ is the mass density. In pSi, the density depends on the porosity ϕ (volume fraction of voids in the layer) as $\rho=\rho_0(1-\phi)$, where ρ_0 is the density of bulk Si. In a solid, the acoustic waves can be longitudinal or transverse. In this letter, only longitudinal waves propagating through pSi are considered, as the waves are coupled into the samples through a liquid at normal incidence. The velocity of the waves is related to the porosity as: $V=V_0(1-\phi)^k$, where V_0=8.43 km s^{-1} (Ref. 6) is the longitudinal velocity of sound in bulk crystalline Si in the (100) direction and $k \geq 0.5$ is a constant. In general, the parameter k depends on pSi morphology which in its turn depends on the doping level of the Si substrate. Multilayer porous structures were electrochemically etched into boron-doped (100)-oriented Si substrates with a resistivity of 10–15 mΩ cm; in this case k=0.58.[7] Room-temperature anodization was performed using a 1:1 solution of 49% HF and ethanol. Pairs of layers in the acoustic DBR were designed to form a half-wave thick layer for the GHz longitudinal acoustic waves. High- and low-porosity layers were obtained by alternating the current density. The physical thickness d_i of the layers was controlled by the etch duration.

Figure 1(a) shows a scanning electron microscope (SEM) image of a typical acoustic pSi multilayer structure. The layer porosity was 47% and 61% with layer thicknesses of 2.2 and 1.7 μm for the alternating layers of pSi. The porosity and thicknesses of the layers were chosen to place the stop bands within the bandwidth of the acoustic transducers. Figure 1(b) (solid line) shows the measured transmittance of a pSi acoustic mirror (24 pairs) with a total thickness of ~94 μm. The gaps in the transmission spectrum observed at 0.65 and 1.3 GHz are the first and second order acoustic stop bands of the mirror, corresponding to m=1,2 in Eq. (2). The fundamental stop band shows an impressive attenuation of ~50 dB with a fractional bandwidth of 33%.

Equations (1) and (2) show that nanostructured multilayered pSi samples can simultaneously exhibit acoustic and

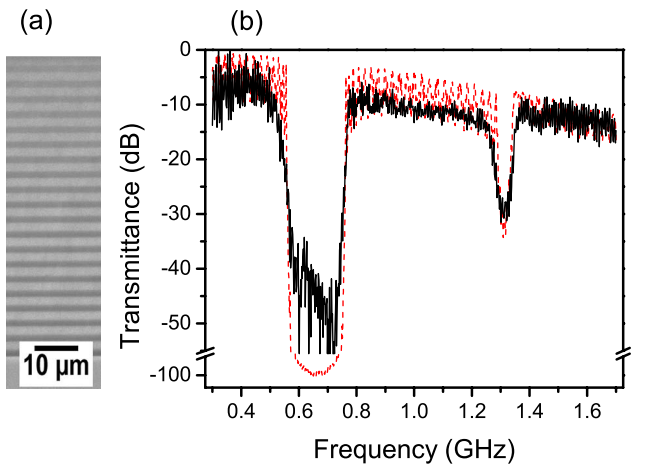

FIG. 1. (Color online) (a) SEM image of pSi DBR. The layers with lower porosity appear brighter. (b) Solid curve: measured acoustic wave transmission spectrum through a pSi DBR. The transmission, recorded on a logarithmic scale, is normalized to its maximum and corrected by an envelope function of the transducers response. Dashed curve: calculated spectrum. See text for details.

[a]Electronic mail: g.aliev@bath.ac.uk.

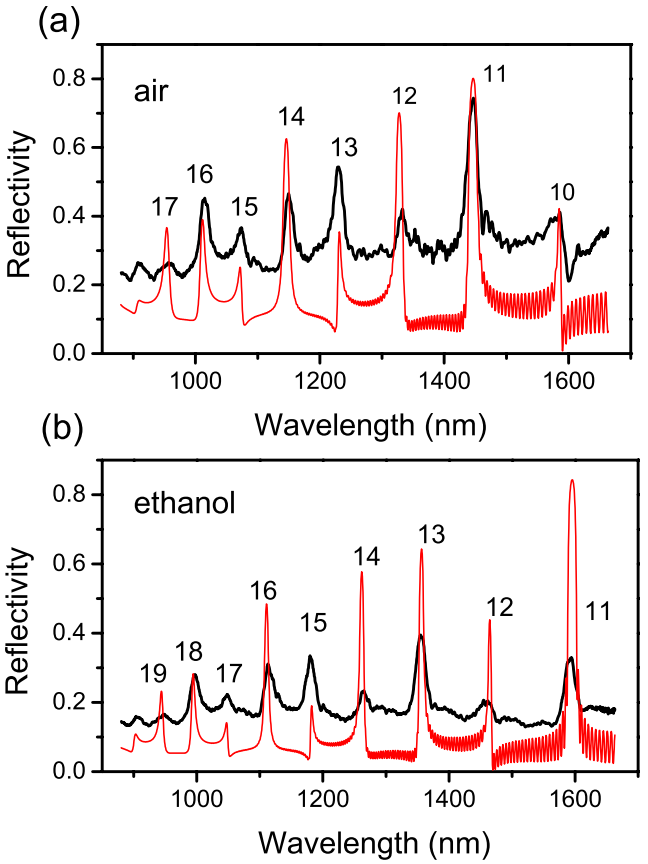

FIG. 2. (Color online) Thick curves: optical reflectivity spectra measured for DBR with pores filled by (a) air and (b) ethanol. Thin curves: the results of fitting procedure using parameters n_i and d_i indicated in the text. Numbers indicate the order m of the optical stop bands.

optical stop bands. Figure 2 shows optical reflectivity spectra for the acoustic DBR shown in Fig. 1, with the pores filled with air or ethanol. The eight reflectivity peaks observed in Fig. 2(a) are high order reflectivity modes for $m=10$ to 17. From Eq. (1), it can be seen that the wavelength of the maxima in the reflectivity allow the optical thickness nd of each layer to be identified. In practice, some uncertainty in the porosity attained during etching and the resolution of thickness measurements, means that the porosity and the thicknesses of the layers cannot be uniquely determined by a single measurement. Hence, the pores of the sample were filled with ethanol ($n=1.35$) (Ref. 8) and the reflectance was measured again as shown in Fig. 2(b) with nine reflectivity peaks ($m=11$ to 19). To model the in-air and in-ethanol spectra consistently, the porosity and the thicknesses of the layers have to be known. The thick curves show measured reflectance spectra while the thin curves in Fig. 2 are the results of calculations. The fitting curves were obtained, using a transfer matrix method, with the following values: $d_1=2.15$ μm for the layer with porosity of 47%, which corresponds to effective refractive indexes $n_1=2.25$ in air and 2.45 in ethanol, and $d_2=1.70$ μm for the layers with porosity of 61% ($n_2=1.85$ in air and 2.12 in ethanol). This gives a fundamental optical band gap for air-filled pores at a wavelength of 15.7 μm. We used the Bruggeman effective medium approximation, which has been shown to be sufficient,[9] to calculate the relation between ϕ and n of pSi. Since the size of the pores (here ~20 nm) is significantly smaller than the wavelengths of our acoustic waves (~5 μm), pSi can be

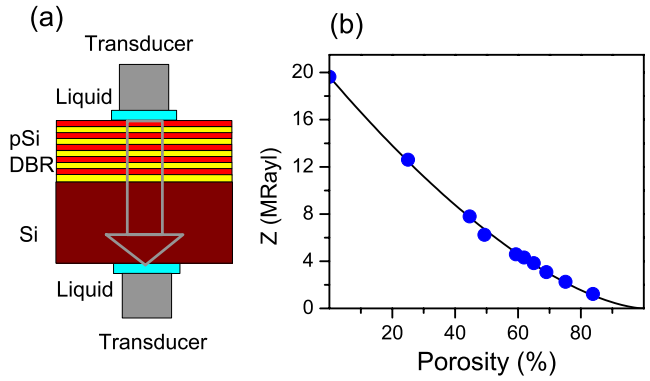

FIG. 3. (Color online) (a) Schematic of experimental setup used for acoustic transmittance measurements. (b) The measured acoustic impedance of pSi for longitudinal waves vs porosity for pSi single-layers. Line is fitted by semiempirical formula. See text for details.

considered as a continuous medium for acoustic waves.

The acoustic transmission spectrum presented in Fig. 1 was measured using the experimental technique described in Ref. 7 [see schematic in Fig. 3(a)] and has been modeled using a transfer matrix method,[10] which includes the effect of the sample, transducers, and liquid coupling the transducers to the sample. At normal incidence for acoustic waves and when only pure longitudinal waves exist, the same matrix method can be used for both optic and acoustic waves by replacing n with the acoustic admittance $1/Z$. The values of porosity and the layer thicknesses used are those obtained from the optical experiment and, therefore, the acoustic band gap can be characterized using the optical results. The result of the modeling is shown in Fig. 1(b). The fine features of the spectrum are not noise but the longitudinal modes of the Si pillars of the transducers and the Si substrate of the sample. Good agreement between modeled and measured spectra is seen. For a perfectly balanced DBR for which each layer has a path length of quarter-wavelength, there are no even-order stop bands. Here, the weaker second order band gap at 1.3 GHz shows that the layers were not balanced. The fundamental band gap has a depth of ~50 dB which is less than the modeled value of ~100 dB. However, this is an experimental artifact as our experimental setup was measuring its noise floor. Thus, we can conclude that the stop band has a depth of at least 50 dB. It should be noted that it was possible to accurately model the depth of the second order stop band. Hence, the results suggest that true depth of the first order acoustic stop band could, in fact, approach 100 dB.

Figure 4(a) shows an SEM image of three pairs of DBR layers ($d_1=1.38$ μm, $\phi_1=0.57$, $d_2=1.53$ μm, $\phi_2=0.40$) cladding a wider high porosity cavity layer ($d_c=2.7$ μm, $\phi_c=0.57$). Figure 4(b) demonstrates the transmission mode at 0.96 GHz within the fundamental stop band ranged from 0.8 to 1.2 GHz (40% fractional bandwidth). The transmission band was deliberately (for demonstration purposes) designed to be rather broad with a full width at half maximum of 33 MHz resulting in a Q-factor of ~30 for the cavity mode. Increasing the number of pairs of layers will lead to narrowing of the transmission band together with deepening of the stop band. The modeled transmittance of the microcavity, using the same transfer matrix method as before, shows a good match to the experimental results [Fig. 4(b)].

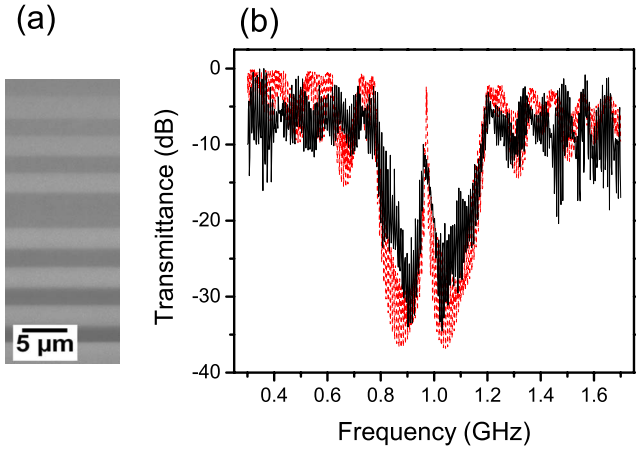

FIG. 4. (Color online) (a) SEM image of acoustic microcavity structure (thickness of ~20 μm). (b) Acoustic longitudinal wave transmission through pSi microcavity structure. Solid curve: measured transmittance spectrum normalized as in Fig. 1. Dashed curve: calculated transmittance.

For commercial acoustic mirrors which are components of solidly mounted resonators and filters,[11] a low-acoustic-impedance material such as SiO_2 is layered with high-impedance materials such as tungsten or molybdenum. It is possible to recast the equations describing a Bragg mirror in terms of the ratio of the impedances between the layers. The peak reflectivity R_B at the center of an acoustic stop band of N layer pairs where the individual layers have impedance Z_1 and Z_2 is defined as follows:

$$R_B = \left[\frac{(Z_2/Z_1)^{2N} - 1}{(Z_2/Z_1)^{2N} + 1} \right]^2. \quad (3)$$

For the layer pair of molybdenum and silica, where $Z^{Mo}=66.2$ MRayl and $Z^{SiO_2}=13.1$ MRayl,[12] the fixed impedance ratio is 5.1. Figure 3(b) shows the measured values of the acoustic impedance of pSi layers versus porosity. The line in Fig. 3(b) exhibits a fit according to the following empirical formula: $Z=Z_0(1-\phi)^{k+1}$, where $Z_0=19.6$ MRayl is the impedance of bulk Si in (100) crystallographic direction, k and ϕ are as defined above. The impedance falls rapidly with increasing porosity as both the density and the velocity of sound decrease in highly porous layers. For a porosity variation of 45% between layers having 30% and 75% porosity, an acoustic impedance ratio of 5.1 can be achieved. Thus, by modulating the porosity of the all-pSi acoustic mirrors, very high reflectivity values can be achieved despite the relatively low acoustic impedance of bulk Si. We would like to note that no aging effects have been observed for the pSi-based acoustic mirrors presented here after 20 months storage in air at ambient temperature and humidity. This suggests that there is no significant change to the acoustic properties of the pSi matrix from slight surface oxidation in ambient conditions.

To conclude, we have demonstrated a Bragg mirror and a microcavity for longitudinal acoustic waves as examples of all-Si one-dimensional phononic crystals. Using optical techniques, the periodicity of the etched structures can be verified in order to predict the acoustic properties. The acoustic mirrors have a performance which is at least comparable with that of current commercial devices.

This work was financially supported by the EPSRC (Project No. EP/C010469/1).

[1] O. Bisi, S. Ossicini, and L. Pavesi, Surf. Sci. Rep. **38**, 1 (2000).
[2] A. Kiuchi, B. Gelloz, A. Kojima, and N. Koshida, *Group-IV Semiconductor Nanostructures*, MRS Symposia Proceedings, No. 832, L. Tsybeskov, D. J. Lockwood, C. Delerue, M. Ichikawa, Eds. (Materials Research Society, Pittsburgh, 2005), p. F3.7.1.
[3] A. Reinhardt and P. A. Snow, Phys. Status Solidi A **204**, 1528 (2007).
[4] G. N. Aliev and P. A. Snow, *Applications of Group IV Semiconductor Nanostructures*, MRS Symposia Proceedings, No. 1145, T. van Buuren, L. Tsybeskov, S. Fukatsu, L. Dal Negro, F. Gourbilleau, Eds. (Materials Research Society, Pittsburgh, 2009), p. MM13.
[5] L. C. Parsons and G. T. Andrews, Appl. Phys. Lett. **95**, 241909 (2009).
[6] H. J. McSkimin and P. Andreatch, Jr., J. Appl. Phys. **35**, 2161 (1964).
[7] G. N. Aliev, B. Goller, D. Kovalev, and P. A. Snow, Phys. Status Solidi C **6**, 1670 (2009).
[8] J. Rheims, J. Köser, and T. Wriedt, Meas. Sci. Technol. **8**, 601 (1997).
[9] W. Theiβ, S. Henkel, and M. Arntzen, Thin Solid Films **255**, 177 (1995).
[10] C. L. Mitsas and D. I. Siapkas, Appl. Opt. **34**, 1678 (1995).
[11] Y. Satoh, T. Nishihara, T. Yokoyama, M. Ueda, and T. Miyashita, Jpn. J. Appl. Phys., Part 1 **44**, 2883 (2005).
[12] A. Briggs, *Acoustic Microscopy* (Clarendon, Oxford, 1992).